A Standalone BLDC Based Solar Air Cooler with MPP Tracking for Improved Efficiency

Sreedhar Madichetty, *Member, IEEE*, Deepak Pullaguram, *Student Member, IEEE*, and Sukumar Mishra, *Senior Member, IEEE*

***Abstract*—This article proposes the idea of using Solar Energy (SE) as a source of power for designing and developing a standalone air-cooling system. This type of application is particularly suited for rural areas that have a considerable amount of solar radiation and have no access to grid systems. The proposed system is comprised of a photovoltaic (PV) array, DC-DC boost converter and DC-DC buck converter. Two Permanent Magnet Brushless Direct Current (PMBLDC) motors are employed to drive a centrifugal water pump and an air blower coupled to their individual shafts. The air blower is connected with a DC-DC boost converter that ensures a maximum power point (MPP) operation. A centrifugal water pump is connected with a DC-DC buck converter. The challenging task in an air cooling system is to maintain the constant speed of the blower under variable irradiance conditions. The power provided by the solar PV array can be shared between the two DC-DC converters in such a way that the BLDC motor connected with the blower will maintain a constant speed by maintaining the constant voltage of the DC-DC boost converter. The rest of the available PV power will be handled by the pump. The suitability of the proposed system for various perturbations is evaluated by simulating the proposed system using a MATLAB/Simulink and is validated by conducting experiments. Case studies have been performed with a variable PV irradiance and the results are explored.**

***Index Terms*—BLDC air blower, BLDC motor, BLDC Pump, PV System.**

I. Introduction

THE rate of energy consumption is increasing very rapidly due to increases in population, industrialization, transportation, etc. and the energy supply is depleting due to the annihilation of fossil fuels, resulting in inflation and energy shortages. This paves the way for exploring other available renewable resources. Among all the renewables, solar is the most abundant and the effective harvest of this energy can easily fulfil the present energy demands of the world [1].

Though the extraction of energy from the sun is a bit costly, the reduction in the cost of power electronic devices and Solar Panels in recent years along with their increased lifetime [2] has increased the usage of solar photovoltaic (PV) based generation for various household and industrial applications.

Although several researches have been carried out on PV array fed automotive and irrigation systems combining various DC-DC converters and motor drives [3]–[6], very little work has been done on PV based home appliances. Further, the applications of BLDC motors are expanding, as these motors are highly reliable, highly efficient, with low radio frequency interference, noise and high torque/inertia ratio with improved cooling, and require practically no maintenance [5], [6]. Due to these merits, a BLDC motor is considered to help develop a solar PV fed air cooler, which can operate satisfactorily for longer time periods as compared to brushed motors under dynamically changing atmospheric conditions. The Perturb & Observe (P&O) based maximum power point tracking (MPPT) algorithm [7] is used to control the DC-DC converter such that the solar PV system always operates at its MPP.

The challenging issue in designing a solar air cooler as compared to solar pumps [4]–[6] is to maintain the constant speed of the motor that drives the air blower. In the process of maintaining the constant speed of the air blower, power imbalance occurs between the PV source and the load which otherwise leads to a continuous rise or fall in the DC capacitor voltage. To avoid this power imbalance and to manage DC voltage within limits, an additional BLDC motor is used which can be used to drive the pump load in the cooler. Two three-phase voltage source inverters (VSI) are used to feed the BLDC motors driving the cooler mechanical loads. The inverters are operated at fundamental frequencies which are obtained from the motor running speed which reduces the switching losses in the inverter [6]. A hall sensor-based scheme is adopted to obtain the speed and position of the BLDC motor [8]. The electronic commutator provides the gate pulses to the inverter circuit and hence controls the pattern of the stator currents of the BLDC motor. An inner hysteresis current controller based speed controller scheme is adopted which controls the motor speed control and also limits the current flowing through the inverter and the BLDC motor which is used to drive the air blower. Further, an optimal power extraction from the SPV system is given in [12]–[14].

This paper is organized as follows: Section II describes the configuration of the solar air cooler system. The designing procedure for individual components of the solar air cooler is illustrated in Section III. Section IV explains the control schematic used for both the BLDC motors along with the DC

Manuscript received March 27, 2018; revised May 15, 2018; accepted May 23, 2018. Date of publication March 30, 2019; date of current version January 21, 2019. This work was supported in part by the DST, Government of India under project "Identification and Demonstration of Cost Effective Technologies to Maximize Habitat Energy Self-sufficiency" with file no. TMD/CERI/BEE/2016/096(G) and NPDF scheme of SERB with file no. SERB/NPDF/2017/000568.

S. Madichetty (corresponding author, e-mail: sreedhar.803@gmail.com), D. Pullaguram, and S. Mishra are with Indian Institute of Technology, Delhi, New Delhi, India.

DOI: 10.17775/CSEEJPES.2018.00410

voltage control. The performance evaluation of the air cooler is described in Section V while being subjected to different perturbations. Section VI provides the experimental analysis and finally Section VII presents the conclusions of the paper.

II. Solar Air Cooler System Configuration

The existing [1] solar air cooler schematic is shown in Fig. 1 and the proposed system configuration is shown in Fig. 2 respectively. The input power is obtained by using a Solar PV panel connected in an array fashion, a DC-DC (boost) converter, along with a voltage source inverter (VSI) and two BLDC motors with an air blower and pump loads coupled to their shafts which are the basic building components of a solar air cooler. The BLDC motor has an inbuilt encoder which encodes the signal generated by the Hall sensors. These signals are sent to the electronic commutator which controls the gate pulses of the inverter feeding the BLDC accordingly. The detailed working operation of the proposed solar air cooler is explained in upcoming sections.

In this system [1], the electrical power generated by the PV system is fed to the motors to drive their respective loads through the DC-DC converter and their respective VSI's. The PV array acts as a power source to the boost converter as shown in Fig. 1. Ideally, the same amount of power shall be transferred at the output of the DC-DC converter as available at the input. But, due to the various losses in the DC-DC converter [2], a slightly lesser amount of the power is feed to the VSI. The Perturb and Observe based Maximum Power Point Tracking (MPPT) controller which has voltage and current sensed from the output of the PV panel as input,

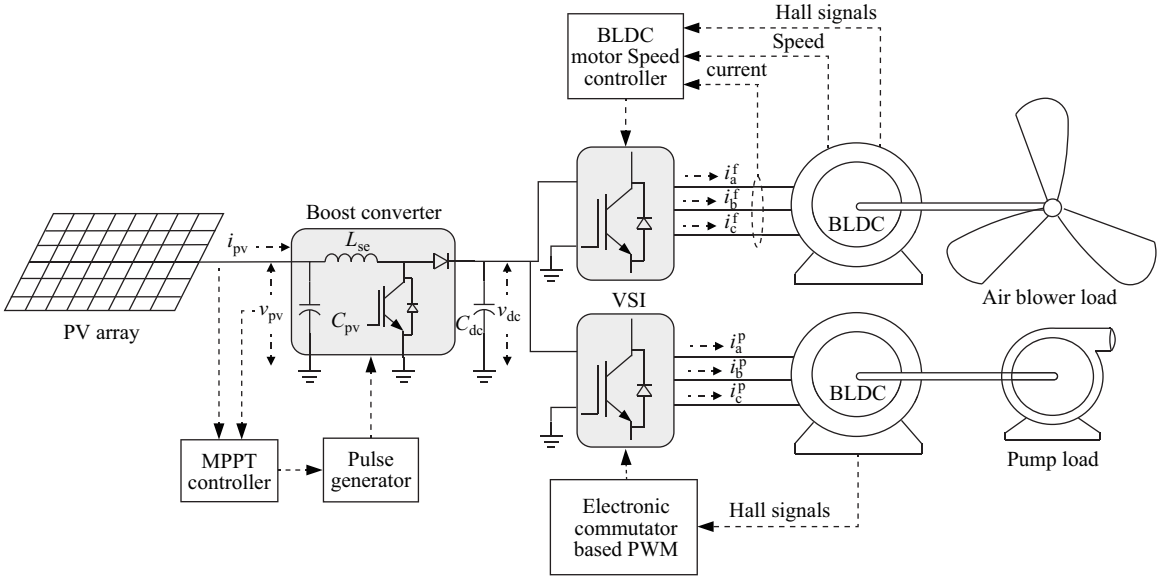

Fig. 1. SPV-Fed Air Cooling System model proposed in [1].

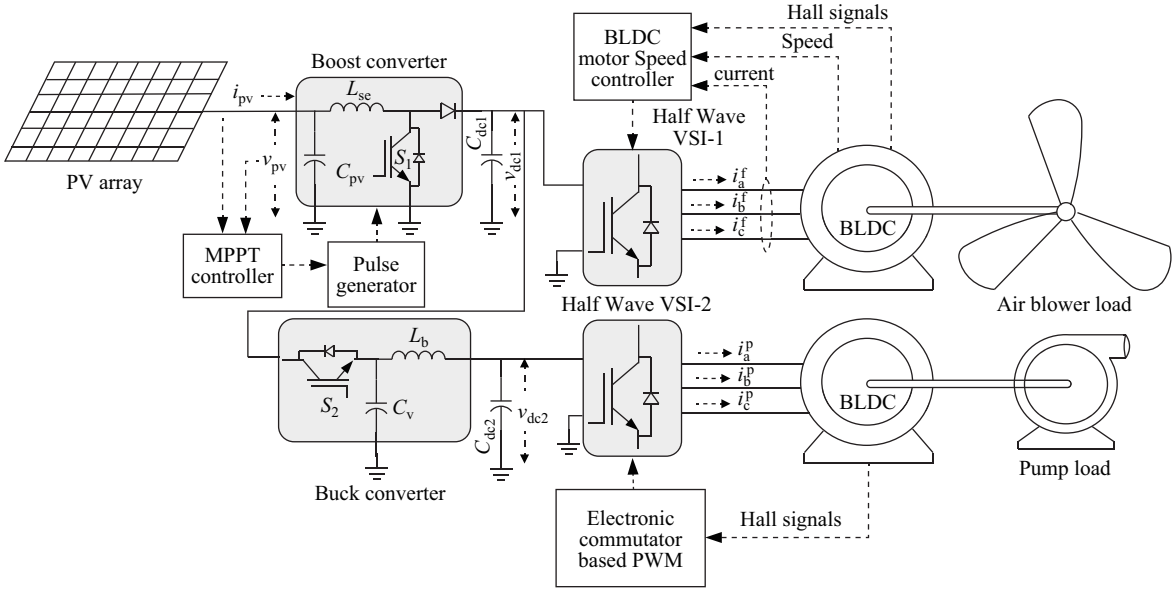

Fig. 2. Modified SPV- Fed Air Cooling System model.

provides the duty cycle to extract the maximum power from the PV system. Furthermore, the VSI of the individual BLDC motors converts the DC input power fed from the DC-DC converter to the AC power that powers up the BLDC motor to drive the centrifugal pump and the blower fan coupled to their respective shafts. The important drawbacks of the proposed converter [1] are, not being able to handle the power sharing properly in the variable irradiance/dynamic conditions. Furthermore, the use of two three phase inverters makes the system so bulky and causes a reduction in its efficiency. Hence, a modified solar air cooling system is proposed with a half bridge voltage source converter. To ensure that the speed of the blower is constant, a stiff voltage is maintained at the end of the boost converter. The detailed operation is provided in Section III.

III. Design of Solar Air Cooler System

For development of an efficient and effective air cooler system that is capable to operate under various uncertain conditions, designing of all the individual components is required. The detailed design of all the considered components such as, half wave VSI, boost converter, buck converter, BLDC motors driving the centrifugal pump and the air blower are described as follows.

A. Design of PV Array with Boost Converter

The proposed SPV array model is designed with two PV modules connected in series. Each PV module has the maximum power voltage $(V_{\rm mp})$ 17.8 V and current $(I_{\rm mp})$ 5.7 A. The PV system is operated at MPPT with the help of the DC-DC converter which is connected across the PV array using the P&O algorithm [7].

The DC-DC converter components such as series inductance $(L_{\rm se})$, input capacitor $(C_{\rm pv})$ and the DC link capacitor $(C_{\rm dc})$ are to be estimated. To reduce the stress on the components, the switch, and converter are always operated in a continuous conduction mode [9]. Therefore for the converter design procedure, the continuous conduction mode is assumed.

For designing the parameters of the boost converter, the maximum switch current needs to be calculated for the minimum input voltage. Therefore, the duty cycle for achieving the maximum switch current is:

$$D = 1 - \frac{V_{\rm mp}\eta}{v_{\rm dc}} \tag{1}$$

where $v_{\rm dc}$, η are the DC output voltage and efficiency of the converter.

In considering the maximum permissible ripple in the rated DC current as 10%, the series inductor $L_{\rm se}$ design can then be given as:

$$L_{\rm se} = \frac{V_{\rm pv} \times (v_{\rm dc} - v_{\rm in})}{\Delta I_{L_{\rm se}} \times f_{\rm sw}} \tag{2}$$

where $\Delta I_{L_{\rm se}}$ is the ripple current allowed through the inductor, and $f_{\rm sw}$ is the switching frequency.

Similarly, the output DC capacitor is designed by considering the maximum allowable voltage ripple $(\Delta v_{\rm dc})$ and operating frequency of the inverter which is obtained from the speed of the BLDC motors. The minimum possible speed of the BLDC motors driving the blower and pump are $\omega_{\rm p}^{\rm min}$ rad/sec and $\omega_{\rm f}^{\rm min}$ rad/sec respectively. The capacitor value can be obtained by:

$$C_{\rm dc} = \frac{i_{\rm dc}}{6 \times \min(\omega_{\rm p}^{\rm min}, \omega_{\rm f}^{\rm min}) \times \Delta v_{\rm dc}} \tag{3}$$

The characteristics of the connected PV panels are given in Fig. 3(a) and Fig. 3(b). The PV panel characteristics are drawn with a constant temperature at 25°C; whereas the irradiance decreases, the output power decreases, which is shown in Fig. 3(a). Furthermore, as the same panels are exposed to various temperature conditions, the temperature increases, and the power delivery capability decreases as shown in Fig. 3(b). The shortcut current, open circuit voltage and maximum peak can be found in the same figures.

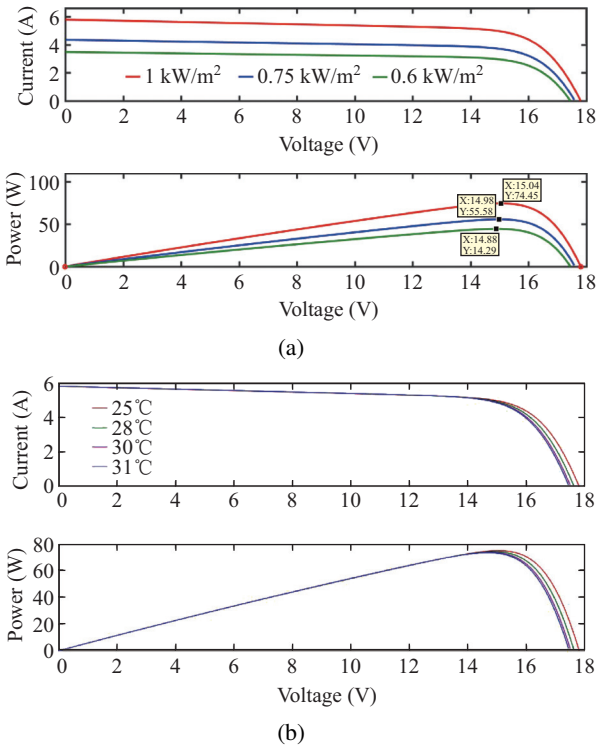

Fig. 3. IV and PV characteristics of a connected PV panel with variable irradiance.

Furthermore, the MPPT is obtained with the P&O algorithm and its flowchart is shown in Fig. 4. Perturb and observe is a linear technique used to track the maximum power point of a system source; in this method, the operating voltage value is regularly increased or decreased based on the direction with respect to current operating voltage location, in order to shift the voltage value towards the maximum power point voltage value.

B. Design of BLDC-motors

Two 3-phase, 4-pole BLDC motors are considered to drive both blower and pump loads. A second-order state-space model that produces a trapezoidal back EMF is used to represent the electrical and mechanical parts of the BLDC motor.

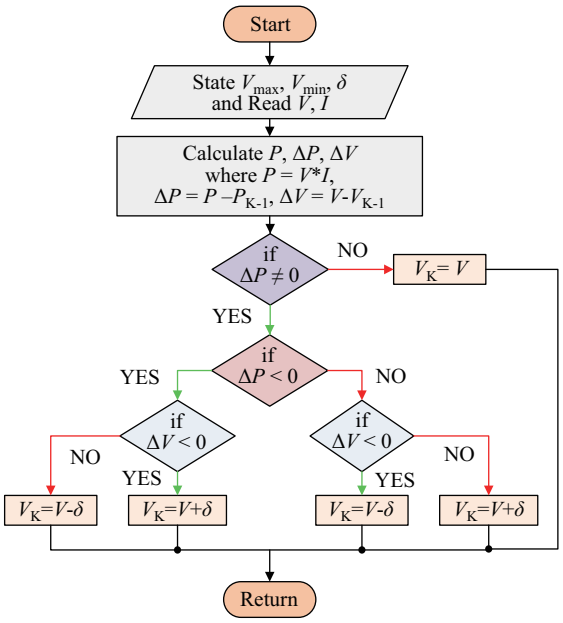

Fig. 4. Implementation of P&OP and O algorithm.

The ratings of the BLDC that drives the blower is set to $0.15HP$ whereas the pump driving the BLDC motor rating is chosen based on the margin of solar irradiance up until when the blower is expected to operate at constant speed. As both the BLDC's are powered by the same PV source, whenever there is a reduction in solar irradiance, the power output of the PV system is also reduced. This causes the blower fan to deviate from its constant speed. During this period, the power supplied to the pump BLDC is curtailed and the maximum possible power is provided to the blower fan BLDC so as to maintain its speed. The proposed system with the BLDC configuration is shown in Fig. 5.

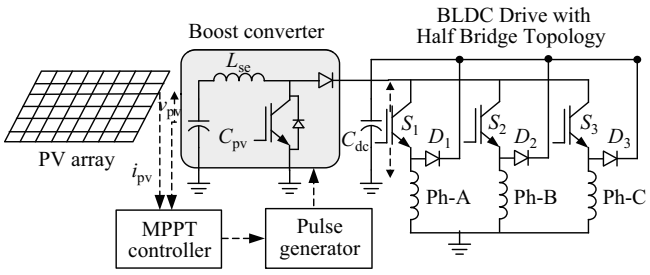

Fig. 5. Proposed topology with DC-DC boost converter.

A three-phase BLDC model is used in the proposed configuration, even though any number of phases can be realized. The BLDC drive can be modeled when phase A is conducting and is given by:

$$V_a = I_a R_a + L_a \frac{\mathrm{d}i_a}{\mathrm{d}t} + E_a \tag{4}$$

$$E_a = k f(\theta)\omega \tag{5}$$

where V_a is the input DC voltage given by the boost converter, I_a is the current flowing through phase-A, R_a is the resistance of the phase-A winding, L_a is the self-inductance, E_a is the phase induced EMF, k is the induced EMF constant,ω is the rotor electrical speed and $f(\theta)$ is a unit function corresponding to the induced EMF of the BLDC as a function of the rotor electrical position. A similar equation can also be valid for Phase-B and Phase-C respectively. With the phase sequence triggering, four modes of operation can be obtained such as motoring, braking, reverse motoring and reverse braking. The function $f(\theta)$ is illustrated in Table I.

TABLE I
UNIT FUNCTION CORRESPONDING TO INDUCED EMF

$f(\theta)$	Angle position
$(\theta)\frac{6}{\pi}$	$0 < \theta < \frac{\pi}{6}$
1	$\frac{\pi}{6} < \theta < \frac{5\pi}{6}$
$(\pi - \theta)\frac{6}{\pi}$	$\frac{5\pi}{6} < \theta < \frac{7\pi}{6}$
-1	$\frac{7\pi}{6} < \theta < \frac{11\pi}{6}$
$(\theta - 2\pi)\frac{6}{\pi}$	$\frac{11\pi}{6} < \theta < 2\pi$

Whereas the other phase functions are displaced at an angle of 120^0. The electromechanical equation with the load is given by:

$$J\frac{\mathrm{d}\omega}{\mathrm{d}t} + B\omega + T_\mathrm{l} = T_\mathrm{e} \tag{6}$$

$$T_\mathrm{e} = k(f_a(\theta)i_a + f_b(\theta)i_b + f_c(\theta)i_c) \tag{7}$$

where J is the moment of inertia, B is the friction co-efficient, T_e is the electromagnetic torque, k is the torque constant and T_l is the load torque. Furthermore, the detailed equation for (3) can be written as:

$$V_a = I_a R_a + L_a \frac{\mathrm{d}i_a}{\mathrm{dt}} + M_{ab}\frac{\mathrm{d}i_b}{\mathrm{dt}} + M_{ac}\frac{\mathrm{d}i_c}{\mathrm{dt}} + E_a \tag{8}$$

$$V_b = I_b R_b + L_b \frac{\mathrm{d}i_b}{\mathrm{dt}} + M_{ba}\frac{\mathrm{d}i_a}{\mathrm{dt}} + M_{bc}\frac{\mathrm{d}i_c}{\mathrm{dt}} + E_c \tag{9}$$

$$V_c = I_c R_c + L_c \frac{\mathrm{d}i_c}{\mathrm{dt}} + M_{ac}\frac{\mathrm{d}i_c}{\mathrm{dt}} + M_{bc}\frac{\mathrm{d}i_b}{\mathrm{dt}} + E_c \tag{10}$$

By combining all the relevant equations, then the system can be written in the state space form as:

$$\left.\begin{aligned} \dot{\boldsymbol{X}} &= \boldsymbol{A}\boldsymbol{X} + \boldsymbol{B}\boldsymbol{U} \\ \boldsymbol{Y} &= \boldsymbol{C}\boldsymbol{X} + \boldsymbol{D} \end{aligned}\right\} \tag{11}$$

where

$$\left.\begin{aligned} \boldsymbol{x} &= [I_a\ I_b\ I_c\ \omega\ \theta]^T \\ \boldsymbol{U} &= [V_a\ V_b\ V_c\ T_l\ 0]^T \\ \boldsymbol{C} &= [\phi\ 1\ 1\ 1\ 1] \\ \boldsymbol{D} &= [0\ 0\ 0\ 0\ 0] \end{aligned}\right\} \pi \tag{12}$$

where

$$\boldsymbol{A} = \begin{bmatrix} -\frac{R_a}{L-M} & 0 & 0 & -\frac{N\phi_a f_a(\theta)}{L-M} & 0 \\ 0 & -\frac{R_b}{L-M} & 0 & -\frac{N\phi_b f_b(\theta)}{L-M} & 0 \\ 0 & 0 & -\frac{R_c}{L-M} & -\frac{N\phi_c f_c(\theta)}{L-M} & 0 \\ \frac{N\phi_a f_a(\theta)}{J} & \frac{N\phi_b f_b(\theta)}{J} & \frac{N\phi_c f_c(\theta)}{J} & \frac{-B}{J} & 0 \\ 0 & 0 & 0 & \frac{P}{2} & 0 \end{bmatrix}$$

$$\boldsymbol{B} = \begin{bmatrix} \frac{1}{L-M} & 0 & 0 & 0 \\ 0 & \frac{1}{L-M} & 0 & 0 \\ 0 & 0 & \frac{1}{L-M} & 0 \\ 0 & 0 & 0 & \frac{1}{L-M} \end{bmatrix}$$

C. Operation of Proposed Converter

The proposed boost converter with a half bridge configuration is shown in Fig. 5. The converter can be obtained by the various switching mechanisms. The switch which is placed in the boost converter can boost the input voltage to the required operating quantity. Thus the obtained voltage is given to the proposed converter drive (air blower). The output voltage of the boost converter is maintained by the capacitor $C_{\rm dc}$. Thus, the obtained voltage can be given to the three phases of the BLDC through S_1, S_2 and S_3. When S_1 is turned ON, the voltage will appear across the Phase-A, which enables it to move into the active region. Some sample modes of operation in conjunction with the boost converter are given in Table II.

TABLE II
OPERATIONAL MODES OF THE HALFBRIDE CONVERTER

Operation Mode	S_B	D_B	S_1	D_1	I_a	I_B
I	ON	OFF	ON	OFF	>0	>0
II	OFF	ON	ON	OFF	>0	>0
III	OFF	ON	OFF	ON	>0	>0

When the boost switch S_B is turned ON, the current starts passing through boost inductor $L_{\rm se}$ and it gets energized. The current and voltage in this mode can be expressed as:

$$V_{\rm dc} = L\frac{{\rm d}i}{{\rm d}t}; \quad i_B > 0 \tag{13}$$

$$I_A = C\frac{{\rm d}V_c}{{\rm d}t}; \quad I_C = -I_A \tag{14}$$

Therefore, the complete voltage equation can be written as:

$$V_{\rm dc} = I_A R_A + L\frac{{\rm d}i_A}{{\rm d}t} + E_a; \quad I_A > 0 \tag{15}$$

By considering the equations from (13) to (15), with the application of boundary conditions, one can find the state space model of the system. By applying the Laplace transform to (15), one can obtain the second order equation as given in (16).

$$I_A(s) = \frac{-sE_a(s)}{S^2L_a + SR_a + \frac{1}{C}} \tag{16}$$

This mode has almost similar second order system characteristics such as natural frequency of the oscillation and damping ratio. Furthermore, the freewheeling modes of the operation for the other two phases can be expressed as:

$$\begin{bmatrix} \frac{{\rm d}I_A}{{\rm d}t} \\ \frac{{\rm d}I_B}{{\rm d}t} \end{bmatrix} = \begin{bmatrix} L_{ab} & M_{ab} \\ M_{ab} & L_{ba} \end{bmatrix}^{-1} \begin{bmatrix} V_{\rm dc} - R_aI_a - E_a \\ -V_{\rm dc} - R_bI_b - E_b \end{bmatrix} \tag{17}$$

The input voltage can be changed at the ON and OFF condition.

D. Design of Blower Fan and Pump Loads

The blower fan and pump loads are designed based on the load torque-speed characteristics. As per these characteristics, both loads exhibit similar torque speed relations [10], [11] which are given by:

$$T_x = k_x\omega_x^2 \tag{18}$$

where $x \in (f, p)$ represents the blower fan and pump respectively, $-\omega$ is the rotor mechanical speed in rad/sec, and T_x- is the centrifugal pump or blower fan load torque. At a steady state, the electromagnetic torque developed by the BLDC motor is equal to the load under steady state operation. For the considered power rating, the value of k_x can be obtained by using:

$$k_x = \frac{P_x}{\omega_x^3} \tag{19}$$

IV. CONTROL SCHEMATIC

The proposed solar air cooling system has two controllers, namely the electronic commutation based control scheme and the speed control scheme for pump and fan load respectively.

A. Electronic Commutation Based Control Scheme

The 120-degree switching logic is one of the most common strategies to control the six-step VSI. In this method, each phase will be conducted two times in one full cycle with a span of 120 electrical degrees each time. Therefore, to have a balanced operation of the BLDC, the hall sensors are spatially placed at 120 degrees apart [8]. Based on the Hall sensor signals, 6 switching pulses are generated as shown in Table III.

TABLE III
SWITCHING STATES FOR ELECTRONIC COMMUTATION OF THE BLDC MOTOR

Hall signal state			EMF of phase			Switching states					
H_a	H_b	H_c	e_a	e_b	e_c	Q_1	Q_2	Q_3	Q_4	Q_5	Q_6
0	0	0	0	0	0	0	0	0	0	0	0
0	0	1	0	-1	$+1$	0	0	0	1	1	0
0	1	0	-1	$+1$	0	0	1	1	0	0	0
0	1	1	-1	0	$+1$	0	1	0	0	1	0
1	0	0	$+1$	0	-1	1	0	0	0	0	1
1	0	1	$+1$	-1	0	1	0	0	1	0	0
1	1	0	0	$+1$	-1	0	0	1	0	0	1
1	1	1	0	0	0	0	0	0	0	0	0

The BLDC VSI's are switched at the fundamental frequency which is obtained by the electronic commutation controller which provides for the Pump-load; the speed of the BLDC-motor is left free and dictated by the additional power available from the PV source, and no external controlling circuit is used to fix the speed, thereby maintaining the power balance, which further maintains the DC link voltage with-in limits. From the above table, the system equations can be derived as:

$$Q_1 = H_a\bar{H}_b\bar{H}_c + H_a\bar{H}_bH_c = H_a\bar{H}_b(\bar{H}_c + H_c) = H_a\bar{H}_b$$
$$Q_2 = \bar{H}_aH_b\bar{H}_c + \bar{H}_aH_bH_c = \bar{H}_aH_b(\bar{H}_c + H_c) = \bar{H}_aH_b$$
$$Q_3 = \bar{H}_aH_b\bar{H}_c + H_aH_b\bar{H}_c = H_b\bar{H}_c(\bar{H}_a + \bar{H}_a) = H_b\bar{H}_c$$
$$Q_4 = \bar{H}_a\bar{H}_bH_c + H_a\bar{H}_bH_c = \bar{H}_bH_c(\bar{H}_a + H_a) = \bar{H}_bH_c$$

$$Q_5 = \bar{H}_a\bar{H}_bH_c + \bar{H}_aH_bH_c = \bar{H}_aH_c(\bar{H}_b + H_b) = H_c\bar{H}_a$$
$$Q_6 = H_a\bar{H}_b\bar{H}_c + H_aH_b\bar{H}_c = H_a\bar{H}_c(\bar{H}_b + H_b) = \bar{H}_cH_a \quad (20)$$

For the three phase, the combinational logic can be obtained as shown in Fig. 5. However, with the usage of a half bridge inverter, the combinational logic circuit will be half and the complexity decreases drastically, at least to half.

B. Speed Control Scheme

The speed of the air blower BLDC motor is controlled by using the control scheme as shown in Fig. 6(a) and its speed controller is given in Fig. 6(b).

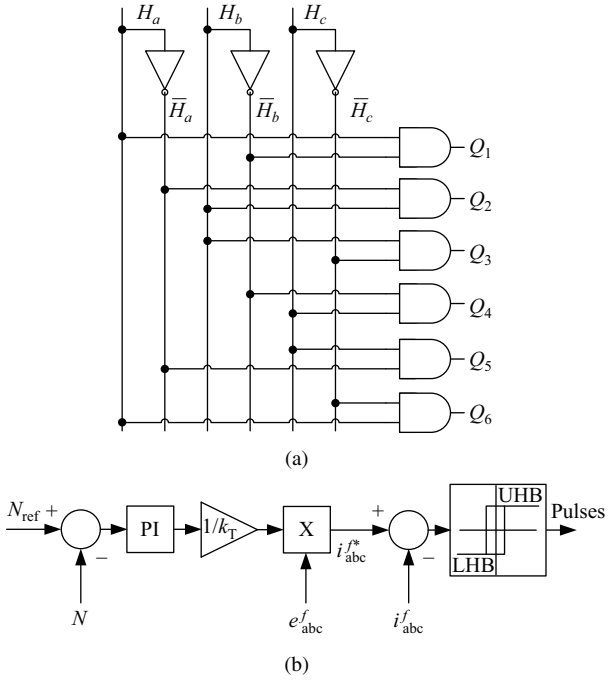

Fig. 6. (a) Combinational logic to implement the six step inverter. (b) BLDC motor speed controller.

For the proposed air blower, a fixed speed is obtained by using the hysteresis control method. It compares the reference speed with the original speed of the BLDC Motor and generates a torque reference which when divided by the machine torque constant 'k_T', gives the current reference magnitude. This current reference magnitude is multiplied with the hall signals generated back EMF $(e^{\mathrm{f}}_{\mathrm{abc}})$ pattern to obtain the current reference $(i^{\mathrm{f}*}_{\mathrm{abc}})$. These current references are then compared with the actual current flowing in the stator through which an error signal is obtained, which is passed through a hysteresis controller that provides the pulses to trigger VSI switches resulting in a desired speed for the air blower fan.

C. DC-link Voltage Controller

If the user wishes to only operate the air blower, in such a case the DC-link voltage increases gradually if no controller is used to restrict it, this happens due to the lack of power balance between the PV source and load. When $P_{\mathrm{pv}} > P_{\mathrm{f}} + P_{\mathrm{loss}}$, the voltage v_{dc} rises progressively. When v_{dc} exceeds a threshold value, there is always a chance that the capacitor and the IGBT switches will be damaged. Therefore, to avoid any damage in the system, the voltage across the DC capacitor is restricted within its safety limits.

To achieve this, there should be a power balance as given by (6) which can be obtained by the DC-rating PV source.

$$P_{\mathrm{pv}} = P_{\mathrm{f}} + P_{\mathrm{loss}} \quad (21)$$

But an exact estimation of the losses is not easy to obtain, so we use the DC voltage control loop in addition to the MPPT control which is enabled when the reaches its threshold. Now, due to the DC-link voltage controller, the voltage across the capacitor is maintained but this causes the PV to operate below MPP. Therefore, less power is extracted but this is not a problem, as the mechanical load required to be driven is also reduced.

V. Results and Discussion

A 230 W solar air cooler model is designed as described in Section III. In this case, both the BLDC's are considered to be of equal rating so that the air blower can be operated at a constant speed up to 500 W/m^2 irradiance. In this scenario, the system behavior for the varying irradiance along with the initial dynamics of the BLDC motors are studied which is portrayed by Fig. 7. Initially the irradiance of the system is at 1000 W/m^2 and the speed reference of the system is maintained constant at 1200 RPM during this case.

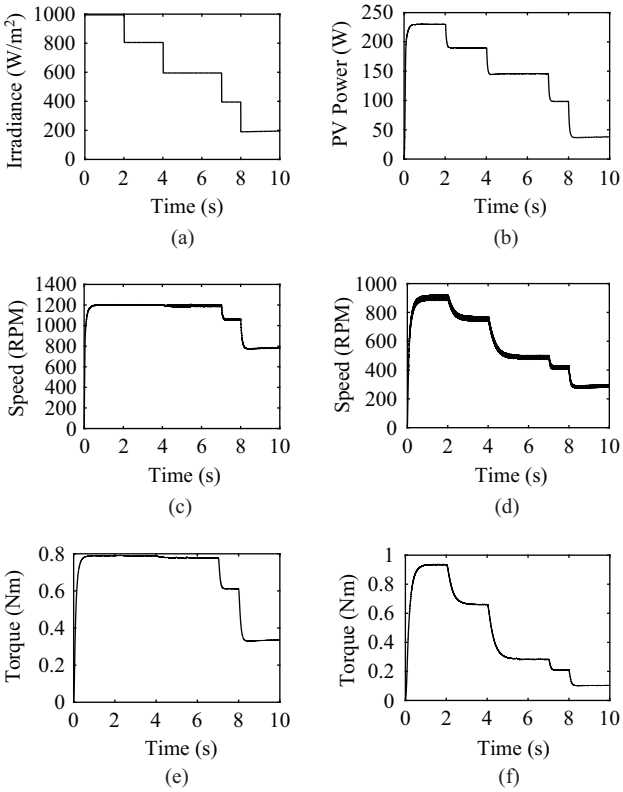

Fig. 7. Performance of solar air cooler for irradiance variation (a) Irradiance, (b) PV power output, (c) Fan speed (d) Pump speed (e) Fan torque (f) Pump torque.

The performance of the proposed air cooler system is assessed by simulating the system in the MATLAB/Simulink

under various conditions. The PV system reached its steady MPP, and both the BLDC motors reached their steady speed within 0.2 sec as shown in Fig. 7. The irradiance is changed in different steps at different times as depicted in Fig. 7(a). As discussed in an earlier section, the speed of the air blower BLDC motor is held constant till the irradiance > 500 W/m^2 as shown in Fig. 7(b). During this period, the speed of the BLDC driving pump sees the change in speed, thereby changing torque. When the irradiance level falls below 500 W/m^2 the air blower is no longer capable of maintaining the speed as the power produced by the PV system is drastically reduced. Therefore, both the BLDC's will be under-utilized when the solar irradiance becomes too low; even though both the motors show the de-rated operation. As the air blower has been given a primitive role, care has been taken to ensure that most of the time it extracts maximum possible power from what's available and the rest of the cases shown in Fig. 7 are self-explanatory.

A. Speed Variation

During this case study, the irradiance of the PV system is held at a constant value of 700 W/m^2. This study details the speed control capability of the BLDC motor that drives the air blower as per the reference value.

Initially the air blower is driven at a constant speed of $1200\ rpm$ extracting maximum possible power from the PV system so as to maintain the reference speed. At $t = 2s$ the speed reference is changed from $1200\ rpm$ to $1100\ rpm$. Immediately the controller action occurs to track the reference value and it reaches to a steady reference speed within 0.2 s. Meanwhile, as the speed is reduced, the load torque, which is proportional to the spare times of the speed, will be reduced which thereby reduces the power consumed by the air blower. To ensure the power balance in the system, the additional power is supplied to the pump system, thereby increasing the speed and torque of the pump load as shown in Fig. 8(c), (d), (e) and (f).

B. DC Voltage Control

This case study provides the details for when the PV power exceeds the power demand. Whenever there is a mismatch in power generated and load, there will be an increase or decrease in the DC voltage.

If $P_{\rm pv} < P_{\rm f} + P_{\rm p}$ then there will be a decrease in voltage which in turn reduces the speed of the BLDC's, thereby reducing the total load on the PV system and achieving a power balance. But this is not the case if $P_{\rm pv} < P_{\rm f} + P_{\rm p}$ and $P_{\rm f}$ is expected to operate at a constant speed while the pump load is OFF. This causes a continuous increase in the $v_{\rm dc}$ as shown in Fig. 9(a) from $t = 1$ s to 1.5 s when the pump load is OFF and rest of the system is being kept unaltered. Hence to avoid any damage due to an increase in the $v_{\rm dc}$ the voltage is restricted to an upper limit of 130 V as shown in Fig. 9(a). As the DC voltage is restricted, the PV is forced to operate at a reduced power level as depicted in Fig. 9(b), while the other components of Fig. 9(c), 9(d), 9(e) and 9(f) are self-explanatory. The stator current, input voltage, induced EMF and torque waveforms are shown in Fig. 9.

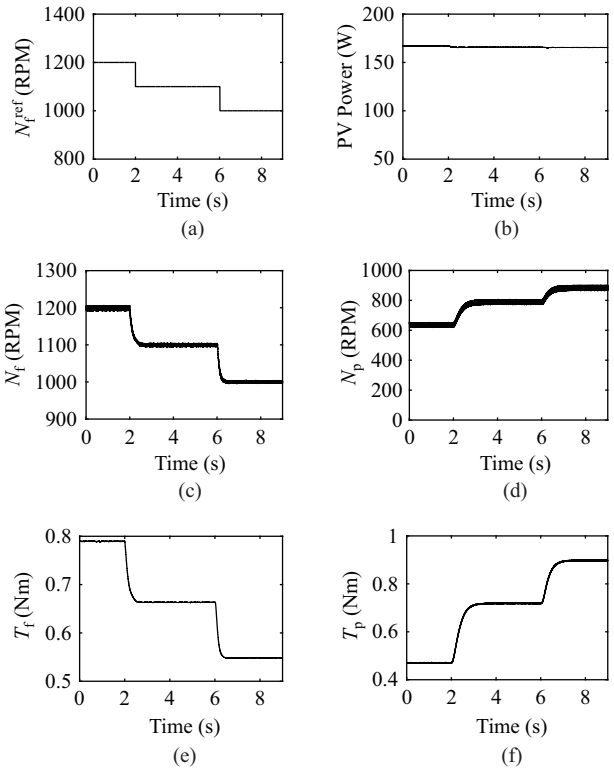

Fig. 8. Performance of the solar air cooler for fan speed reference variation (a) Fan speed reference, (b) PV power output, (c) Fan speed (d) Pump speed (e) Fan torque (f) Pump torque.

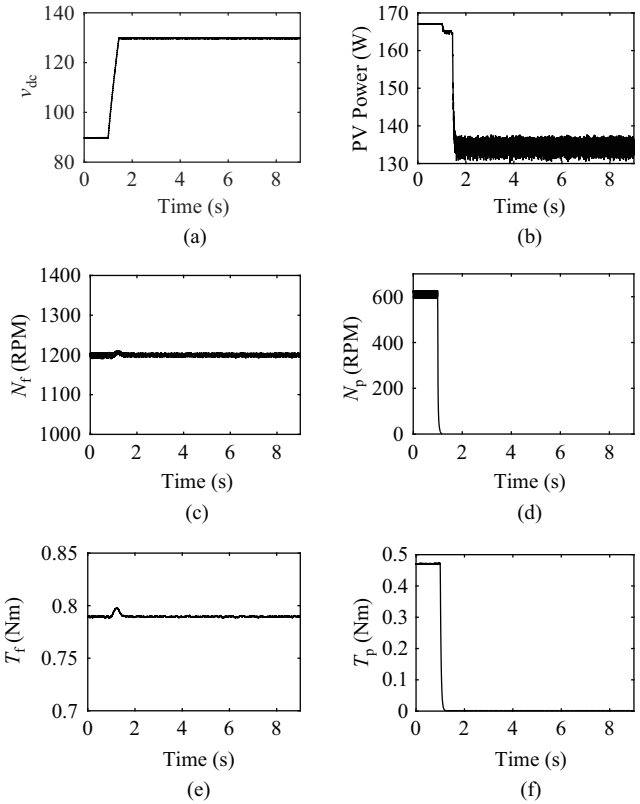

Fig. 9. Performance of the solar air cooler when pump is off (a) DC voltage, (b) PV power output, (c) Fan speed (d) Pump speed (e) Fan torque (f) Pump torque.

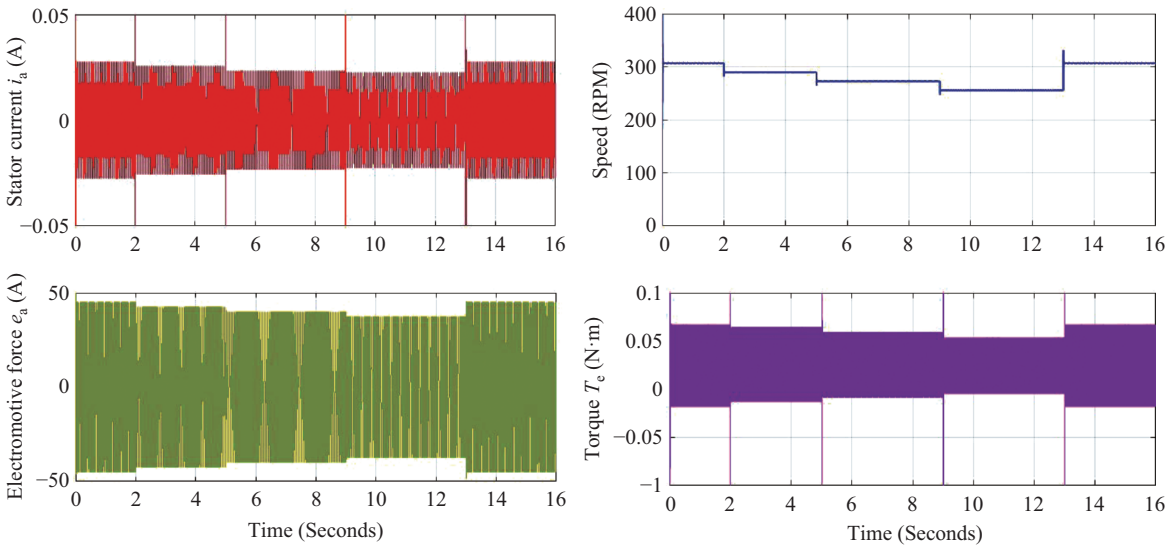

Fig. 10. Performance of PV with variable DC voltage control.

VI. Experimental Analysis

The proposed system is tested by conducting experiments under various conditions such as variable irradiance and variable input voltage.

The experimental system consists of two PV arrays, each with ratings of 100 W at 1000 W/m^2 irradiance. These are connected in series with an open circuit voltage of 36 V. The fan blower is supplied with 90 V input DC voltage (which can vary up to 110 V DC) with a provided boost converter. The reason that the PV interconnection is needed for the boost converter is to enhance the speed horizon of the BLDC. This function of the boost converter is determined based on the MPPT algorithm. As the objective is to maintain the speed of the blower, the output voltage of the boost converter is maintained at constant and the speed is thereby maintained. The parameters of the pump and BLDC are provided in Table IV.

TABLE IV
Parameters Used in Experimentation

Parameter	Value
Stator Phase resistance	2.875 Ohms
Stator Phase inductance	8.5 mH
Flux Linkage	0.35 vs
Viscous Damping	0.001 Nm-s
Inertia	0.008 kg-m2
Pole pairs	4
Back EMF	Trapezoidal

The system is investigated with variable irradiance, partial shading conditions and its results are shown in Fig. 10. The experimental setup of the proposed system is shown in Fig. 11. As the input irradiance increases, the PV power increases and is shown in Fig. 12(a). Now, the system is subjected to variable irradiance i.e., it initially decreases and then increases. Even though for dynamical changes in the irradiance, the boost output voltage is maintained at constant, this in turn maintains the speed of the BLDC as constant, which is shown in Fig. 12(b). Then the system is subjected to a partial shading

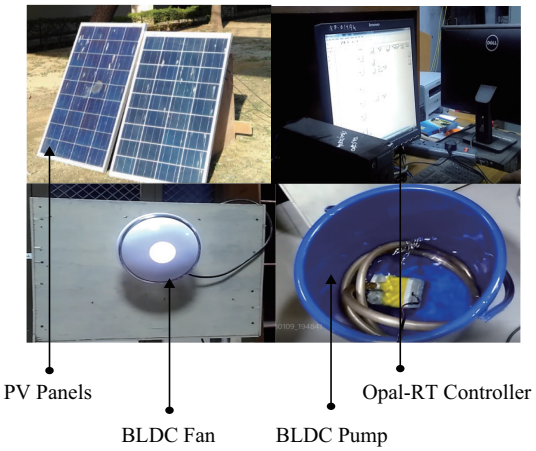

Fig. 11. Experimental setup of proposed system.

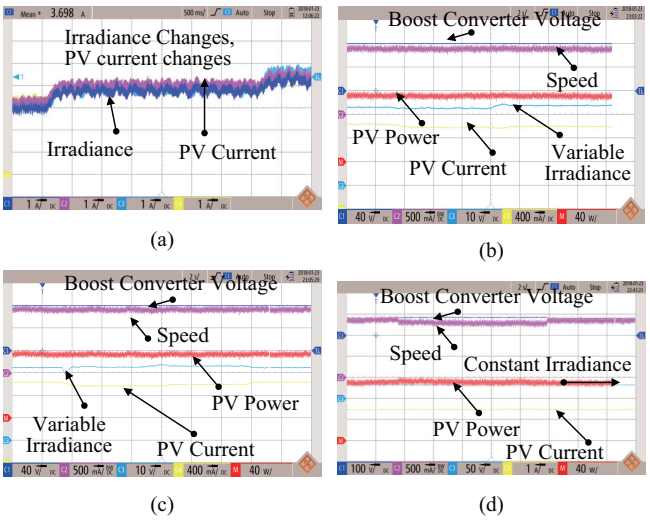

Fig. 12. Experimental results at variable conditions

condition by creating some artificial shadows on the PV panel. Even in this condition, the system maintains the constant boost converter voltage which in turn maintains the speed of the BLDC and the rest of the power is given to the BLDC. This is shown in Fig. 12(c). Furthermore, the boost converter voltage is reduced with the control, which in turn reduces the speed of the BLDC; however the system is maintained at the MPPT shown in Fig. 12(d). From the experimental analysis, it is clear that the system is maintained at the MPPT under variable irradiance conditions and delivers the power as per the requirements.

VII. Conclusion

A solar standalone air-cooling system using a pair of BLDC motors to drive the pump and air blower fan load coupled to their individual shafts is implemented in MATLAB/Simulink and then verified by conducting an experiment. The maximum power point (MPP) operation of the photovoltaic (PV) array obtained with a DC-DC boost converter which is adjoined with the DC voltage control so as to ensure safe operation during light load conditions and the DC-DC buck converter ensures the proper operation of the pump. The speed of the air blower system is maintained constant with the help of the pump load, although there is variation in the solar irradiance. Furthermore, the speed controller is used to vary the speed of the air blower as per the user requirements and ensuring its ability to extract maximum possible power from the PV system.

References

[1] D. Pullaguram, S. Mishra, and S. Banerjee, "Standalone BLDC based solar air cooler with MPPT tracking for improved efficiency," in *Proceedings of the 7th Power India International Conference*, Bikaner, pp. 1–5, 2016, doi: 10.1109/POWERI.2016.8077370.

[2] Lewis NS, Crabtree G. "Basic research needs for solar energy utilization: Report of the basic energy sciences workshop on solar energy utilization", DOESC, US, 2005.

[3] U. Pillai, "Drivers of cost reduction in solar photovoltaics," *Energy Economics*, vol. 50, pp. 286–293, 2015.

[4] S. R. Bhat, A. Pittet, and B. S. Sonde, "Performance optimization of induction motor-pump system using photovoltaic energy source," *IEEE Transactions on Industry Applications*, vol. IA-23, no. 6, pp. 995–1000, Nov. 1987.

[5] S. Jain, R. Karampuri, and V. T. Somasekhar, "An integrated control algorithm for a single-stage PV pumping system using an open-end winding induction motor," *IEEE Transactions on Industrial Electronics*, vol. 63, no. 2, pp. 956–965, Feb. 2016.

[6] B. Singh and R. Kumar, "Simple brushless DC motor drive for solar photovoltaic array fed water pumping system," *IET Power Electronics*, vol. 9, no. 7, pp. 1487–1495, Jun./Aug. 2016.

[7] R. Kumar and B. Singh, "BLDC motor-driven solar PV array-fed water pumping system employing zeta converter," *IEEE Transactions on Industry Applications*, vol. 52, no. 3, pp. 2315–2322, May/Jun. 2016.

[8] T. Esram and P. L. Chapman, "Comparison of photovoltaic array maximum power point tracking techniques," *IEEE Transactions on Energy Conversion*, vol. 22, no. 2, pp. 439–449, Jun. 2007.

[9] P. Alaeinovin and J. Jatskevich, "Hall-sensor signals filtering for improved operation of brushless DC motors," in *Proceedings of 2011 IEEE International Symposium on Industrial Electronics*, Gdansk, 2011, pp. 613–618.

[10] D. D. C. Lu, D. K. W. Cheng, and Y. S. Lee, "A single-switch continuous-conduction-mode boost converter with reduced reverse-recovery and switching losses," *IEEE Transactions on Industrial Electronics*, vol. 50, no. 4, pp. 767–776, Aug. 2003.

[11] W. V. Jones, "Motor selection made easy: choosing the right motor for centrifugal pump applications," *IEEE Industry Applications Magazine*, vol. 19, no. 6, pp. 36–45, Nov./Dec. 2013.

[12] A. Lelkes and M. Bufe, "BLDC motor for fan application with automatically optimized commutation angle," in *Proceedings of the 35th Annual Power Electronics Specialists Conference*, Aachen, 2004, pp. 2277–2281.

[13] B. Yang, T. Yu, H. C. Shu, X. S. Zhang, K. P. Qu, and L. Jiang, "Democratic joint operations algorithm for optimal power extraction of PMSG based wind energy conversion system", *Energy Conversion and Management*, vol. 159, pp. 312–326, Mar. 2018.

[14] B. Yang, T. Yu, H. C. Shu, Y. M. Zhang, J. Chen, Y. Y. Sang, and L. Jiang, "Passivity-based sliding-mode control design for optimal power extraction of a PMSG based variable speed wind turbine", *Renewable Energy*, vol. 119, pp. 577–589, Apr. 2018.

Sreedhar Madichetty (M'16) received his B.Tech. degree from Jawaharlal Nehru Technological University, Anantapur, Anantapuramu, India, in 2010, and his M.Tech (topper and gold medalist) and Ph.D. degrees from the KIIT University, Bhubaneswar, India, in 2012 and 2015, respectively. In 2014, he joined the Department of Electrical and Electronics Engineering, Birla Institute of Technology and Science, Pilani as a Lecturer. He is currently a Postdoctoral Fellow with the Department of Electrical Engineering, Indian Institute of Technology, Delhi, New Delhi, India. His research interests include power electronics, power system studies, and renewable energy.

Deepak Pullaguram (S'15) received his M. Tech. degree in power and energy systems from the National Institute of Technology Warangal, India, in 2012. He is currently working toward his Ph.D. degree at the Indian Institute of Technology, Delhi, New Delhi, India. His research interests include Renewable Energy system dynamics and AC/DC microgrid systems.

Sukumar Mishra (M'97–SM'04) received the B.E. degree from the University College of Engineering, Burla, India, in 1990, and the M.E. and Ph.D. degrees from Regional Engineering College, Rourkela, India, in 1992 and 2000, respectively. He is currently a Professor with the Department of Electrical Engineering, Indian Institute of Technology, New Delhi, India. He is working as a National Thermal Power Corporation (NTPC) Chair Professor and has previously worked as the Power Grid Chair Professor, New Delhi. He is also serving as an Independent Director with the Cross-Border Power Transmission Company Ltd, Gurugram, India and an Industry Academic Distinguish Professor. His research interests include power systems, power quality studies, and renewable energy. Dr. Mishra is also a fellow of the IET (U.K.), National Academy of Sciences, India (India), Indian National Academy of Engineering (INAE) (India), Institution of Engineers, India (India), and Institution of Electronics and Telecommunication Engineers (India).